Kinetic pathways leading to layer-by-layer growth from hyperthermal atoms: A multibillion time step molecular dynamics study

D. Adamović,[1] V. Chirita,[1] E. P. Münger,[1] L. Hultman,[1] and J. E. Greene[2]
[1]*Department of Physics, Chemistry and Biology, IFM Linköping University, SE-581 83 Linköping, Sweden*
[2]*Materials Science Department and the Frederick Seitz Materials Research Laboratory, University of Illinois, Urbana, Illinois 61801, USA*

(Received 31 January 2007; revised manuscript received 11 June 2007; published 14 September 2007)

We employ multibillion time step embedded-atom molecular dynamics simulations to investigate the homoepitaxial growth of Pt(111) from hyperthermal Pt atoms (E_{Pt}=0.2–50 eV) using deposition fluxes approaching experimental conditions. Calculated antiphase diffraction intensity oscillations, based on adatom coverages as a function of time, reveal a transition from a three-dimensional multilayer growth mode with $E_{Pt}<20$ eV to a layer-by-layer growth with $E_{Pt}\geq 20$ eV. We isolate the effects of irradiation-induced processes and thermally activated mass transport during deposition in order to identify the mechanisms responsible for promoting layer-by-layer growth. Direct evidence is provided to show that the observed transition in growth modes is primarily due to irradiation-induced processes which occur during the 10 ps following the arrival of each hyperthermal atom. The kinetic pathways leading to the transition involve both enhanced intralayer and interlayer adatom transport, direct incorporation of energetic atoms into clusters, and cluster disruption leading to increased terrace supersaturation.

DOI: 10.1103/PhysRevB.76.115418 PACS number(s): 81.15.Aa, 68.55.Ac, 81.15.Jj, 47.11.Mn

I. INTRODUCTION

Low-energy ion irradiation during film deposition is an effective experimental technique for altering the growth mode from three-dimensional (3D) multilayer growth toward two-dimensional (2D) or layer-by-layer growth and is known to increase the epitaxial thickness of films deposited at low temperatures.[1–8] Several models have been proposed to explain the observed growth mode transition. For example, it has been suggested that incident ions are responsible for suppressing 3D multilayer formation by removal of atoms from stable nuclei during nucleation on upper terraces.[2] It has also been proposed that in the case of Si(001) homoepitaxy, ion bombardment enhances adatom number densities via disruption of dimers, which, in turn, results in higher island nucleation rates.[3] Another explanation is that during bombardment, adatoms created via displacement of surface atoms form adatom islands close to the impact site, thus leading to increased island number densities.[1]

Clearly, the detailed pathway by which low-energy incident ions alter film growth kinetics and surface morphological evolution is complex and not fully understood. This provides a strong incentive for further atomic-scale investigations of the interactions among incident ions and surface atoms. Such energetic impact-induced events are nonequilibrium transient processes which are completed over time scales of order of picoseconds. Thus, they are not easily accessible to direct observation even by state-of-the-art *in situ* experimental techniques which only probe initial and final states. However, computer simulations, in particular, molecular dynamics (MD) simulations,[9–14] allow the direct observation of these events as a function of time.

Here, we present the results of a multibillion time step MD study of the homoepitaxial growth of Pt(111) from hyperthermal atoms with energies E_{Pt}=0.2–50 eV. Given the ability of MD techniques to follow individual atoms on the picosecond time scale, we separate the effects of irradiation-induced processes during deposition from thermally activated mass transport. We find that for all E_{Pt} values, irradiation-induced displacement events are completed within several picoseconds following impacts, a time scale over which thermal migration is not significant. With $E_{Pt}\leq 15$ eV, we observe 3D multilayer growth. However, using the same deposition conditions, but with E_{Pt}=20–50 eV, we obtain 2D growth approaching layer-by-layer growth. Moreover, we provide direct evidence that the transition from 3D to 2D growth is due to the atomistic processes induced during the initial ~10 ps following impacts. The results presented here have increased significance in the low-temperature deposition regime where thermally activated processes are exponentially suppressed.

II. METHOD

In our simulations, we use the embedded-atom method (EAM) parametrization of Johnson,[15] with time steps of 1 fs, to calculate Pt-Pt interactions. This interaction potential yields Pt(111) surface diffusion activation energies for Pt adatoms and small clusters[16] in good agreement with experimental values[17,18] and has been successfully employed in previous studies.[9,10,16,19–23] In addition, we have carried out a number of tests in which we compare the forces among atoms generated in EAM-MD simulations with those obtained in *ab initio* MD simulations using the Vienna *ab initio* simulation package (VASP) code. The results show that for the Johnson EAM parametrization, the magnitudes of interatomic forces are within 15% of those obtained with VASP-MD.

Our Pt(111) substrates consist of nine layers, 16×18 atoms each, with the bottom layer fixed and the two layers directly above it serving as a heat reservoir. The atoms in the remaining layers are allowed to interact freely according to

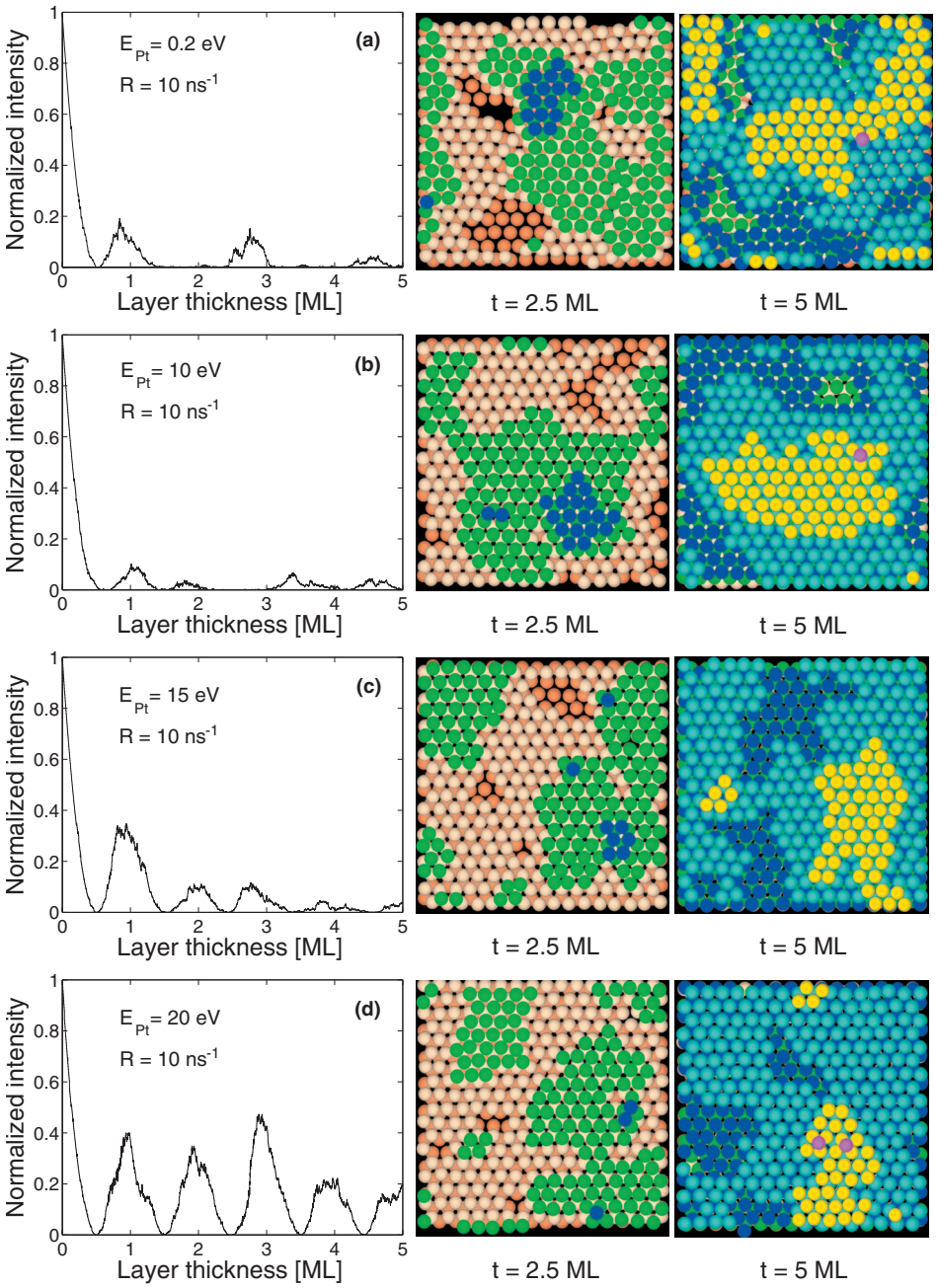

FIG. 1. (Color) Left side: Normalized antiphase diffraction scattering intensity vs deposited layer thickness during Pt(111) homoepitaxy using Pt atoms with incident energies E_{Pt} of (a) 0.2 eV (thermal deposition), (b) 10 eV, (c) 15 eV, and (d) 20 eV. The deposition rate R is 10 ns^{-1}. Right side: Plan-view images showing the corresponding Pt(111) surface topographies after deposition of 2.5 and 5.0 ML. Atoms in the first, second, third, and fourth deposited layers are brown, yellow, green, and blue, respectively.

the EAM potential. Periodic in-plane boundary conditions are employed along orthogonal $[1\bar{1}0]$ and $[\bar{1}\,\bar{1}2]$ directions.

Single hyperthermal Pt atoms, with trajectories perpendicular to the initially flat surface, are introduced into the simulation at randomly chosen points. In addition to the case for which the incident kinetic energy E_{Pt}=0.2 eV (thermal deposition), which serves as a reference, simulations were carried out with E_{Pt} ranging from 5 to 50 eV at 5 eV intervals. We initially deposit 5 ML (monolayer) using each E_{Pt} value and an arrival rate of one atom every 100 ps, for a total simulation time of 1.65 μs. This flux corresponds to a deposition rate of 5×10^5 μm/min, which is 10^3 times higher than typical rates during electron beam evaporation.[24] In a separate MD run, we deposit 5 ML with E_{Pt}=25 eV, but at a flux of one atom every 1 ns, which is only 2 orders of magnitude higher than experimental deposition rates. This MD run, which required a total simulation time of 1.5 μs (1.5×10^9 time steps), represents an attempt to simulate deposition in a fully deterministic manner using fluxes approaching experimental values. We choose a substrate temperature of 1000 K, corresponding to a homologous temperature[8] of $\sim$0.5, to allow for an effective dissipation of excess kinetic energy due to artificially high deposition rates via the heat reservoir. The MD runs are stored in movie files with a 1–2 ps time resolution.

III. RESULTS

Figure 1 shows calculated normalized antiphase diffraction intensities[13] as a function of time during Pt(111) deposition using E_{Pt}=0.2, 10, 15, and 20 eV. The intensity oscillations are similar to those that would be measured by, for

example, reflection high-energy electron diffraction (RHEED). During ideal layer-by-layer growth, new layers start to be formed only *after* the preceding layer is completed.[25,26] Thus, RHEED oscillations during *ideal* layer-by-layer growth maintain constant amplitude. The degree to which an actual growth process approaches ideal layer-by-layer is characterized by the inverse decay rate of the oscillation amplitude.[27–29] In practice, any growth process giving rise to a significant number of oscillations is termed "layer-by-layer."[26] Plan-view images of the atomic-scale surface topographies of the deposited layers after deposition of 2.5 and 5 ML are also presented. The results illustrate several clear features. In Fig. 1(a), the diffraction pattern corresponding to E_{Pt}=0.2 eV growth (thermal deposition) displays weak aperiodic oscillations indicative of 3D multilayer growth. This is consistent with the plan-view image showing substantial fractions of unoccupied lattice sites in the first and second layers (brown and yellow atoms, respectively), while a large island (blue) has already nucleated on top of the third layer (green). In ideal layer-by-layer growth, the first two layers would be completely filled, while the third layer would be half full with no atoms on top. We also observe diffraction intensity oscillations and surface topographies similar to those shown in Fig. 1(a) for Pt growth at E_{Pt}=5 eV (not shown) and 10 eV [Fig. 1(b)].

Increasing E_{Pt} to 15 eV [Fig. 1(c)] yields periodic diffraction oscillations with higher amplitudes, signaling the onset of a transition in growth mode. With E_{Pt}=20–50 eV, strong periodic diffraction intensity oscillations are observed, as shown in Fig. 1(d) for E_{Pt}=20 eV, indicative of layer growth under conditions more closely approximating the 2D layer-by-layer mode. The corresponding 2.5 ML image from our movie files also exhibits a surface topography which is close to ideal layer-by-layer growth, i.e., an almost completely filled second layer with only a few atoms on top of the third, nearly half-filled, layer.

In order to elucidate the primary mechanisms responsible for the observed transition from 3D multilayer to 2D growth, we utilize the capability of MD to monitor individual atomic migration paths during deposition. We first divide the 100 ps between incident Pt impacts into ten intervals of 10 ps each during which the migration distances of deposited and substrate atoms are quantified for the entire duration of the MD run in the following manner. Pt atoms with a net lateral motion $\geq$1.6 Å, i.e., the distance l between adjacent fcc and hcp surface sites on Pt(111), contribute to intralayer migration, while atoms with a net vertical motion $\geq$2.2 Å, which is equivalent to the interlayer spacing d in the [111] direction, are counted as contributing to interlayer migration. Average intra- and interlayer migration distances resulting from each Pt impact are determined for all 10 ps time intervals. This procedure is repeated for each value of E_{Pt}.

Average intralayer and interlayer Pt migration distances, in units of l and d, respectively, for ten consecutive 10 ps time intervals during film growth using thermal (0.2 eV) and 5, 25, and 50 eV hyperthermal atoms are presented in the form of histograms in Fig. 2. The results clearly demonstrate that both intra- and interlayer mass transport are dominated by events occurring during the initial 10 ps and are strongly dependent on E_{Pt}. In contrast, average migration distances

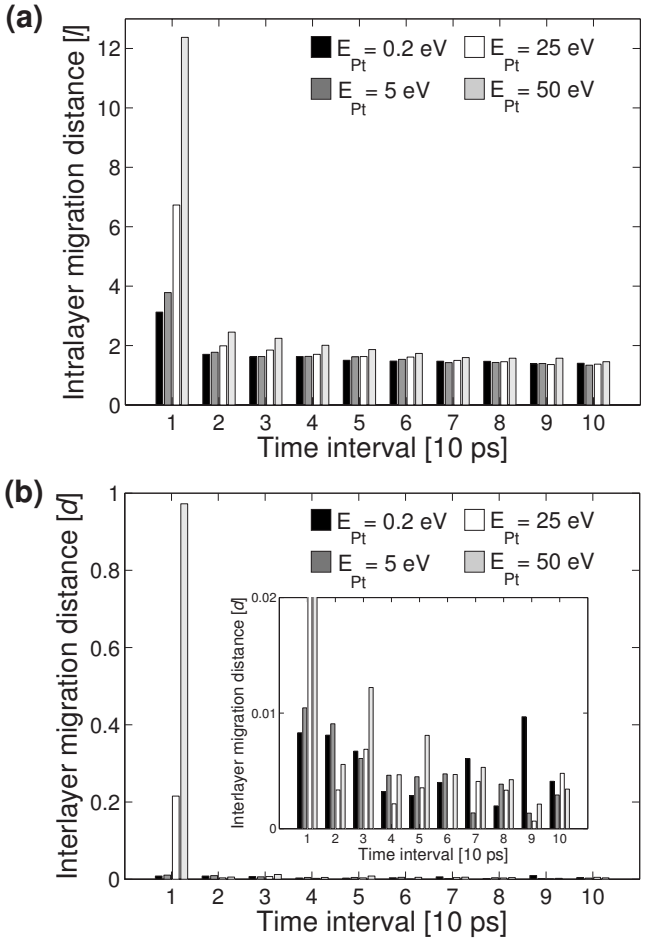

FIG. 2. [(a) and (b)] Histograms showing averaged intra- and interlayer mass transport distances per atom during consecutive 10 ps intervals following the deposition of a Pt atom with E_{Pt} =0.2, 5, 25, and 50 eV on Pt(111). Mass transport values are expressed in units of l, the separation between adjacent fcc and hcp surface sites, and d, the interlayer spacing in the [111] direction.

over the next nine 10 ps intervals are essentially independent of E_{Pt}, indicative of thermally activated diffusion, and are significantly reduced. Note that there is very little *thermally* activated *interlayer* migration during the 100 ps time period between Pt deposition events on Pt(111) at 1000 K. Since the dominant irradiation-induced processes during film growth from hyperthermal species occur during the 10 ps following each bombardment event, we focus on that period in the following discussion.

As a measure of the importance of irradiation-induced mass transport as a function of E_{Pt}, we list in Table I the ratios ρ between migration distances over the initial 10 ps intervals and the corresponding distances during the subsequent 90 ps (the next nine 10 ps periods) following each deposition event. ρ_{intra} and ρ_{inter} in columns 2 and 4, respectively, are the ratios for intra- and interlayer migration. The results clearly demonstrate that irradiation-induced migration is significant even at the lowest deposition energy, E_{Pt} =5 eV, for which both ρ_{intra} and ρ_{inter} are 0.27. ρ increases with increasing E_{Pt} such that at E_{Pt}=50 eV, ρ_{intra}=0.75 and ρ_{inter}=19.3. The trend is even more dramatic if one considers

TABLE I. Calculated ratios of intra- and interlayer mass transport distances during the first 10 ps following each deposition event with E_{Pt}=5, 25, and 50 eV to the total (ρ) and average (r) migration distances over the subsequent 90 ps.

Impact energy E_{Pt} (eV)	Intralayer mass transport		Interlayer mass transport	
	ρ_{intra}	r_{intra}	ρ_{inter}	r_{inter}
5	0.27	2.47	0.27	2.45
25	0.47	4.19	7.49	67.57
50	0.75	6.75	19.34	174.05

the ratios r of irradiation-induced migration to *average* thermal mass transport distances. r_{intra} and r_{inter} (columns 3 and 5 in Table I) range from 2.47 and 2.45 with E_{Pt}=5 eV to 6.75 and 174.05 with E_{Pt}=50 eV.

Detailed results for average intra- and interlayer mass transport during the initial 10 ps following each deposition event for all E_{Pt} values $\geq$5 eV are presented in Fig. 3 as histograms. The intralayer mass transport distance [Fig. 3(a)] increases nearly linearly with E_{Pt}. Since it is possible in MD to follow individual atomic motion, we have identified the thermal component of mass transport (i.e., that due to atoms not directly involved in collision events) during the irradiation period and plotted this as the dashed line in Fig. 3(a). Even after accounting for this component, we still find that increasing E_{Pt} from, for example, 10 to 20 eV increases the average intralayer migration distance by a factor of almost 2. This is primarily due to increases in adatom scattering distances and the onset of cluster disruption. Figure 3(b) shows that irradiation-induced interlayer transport becomes significant with $E_{Pt}\geq$15 eV, where we again observe a near linear dependence between the average migration distance and E_{Pt} with d values ranging from 0.05 with E_{Pt}=15 eV to 0.95 with E_{Pt}=50 eV.

The increased intra- and interlayer adatom migration distances are the only notable changes in our MD simulations with increasing E_{Pt} and are responsible for the observed transition in film growth mode from 3D multilayer to 2D growth which occurs at $E_{Pt}\approx$20 eV. From following individual impact events,[9,10] we observe that adatom scattering, surface channeling, and cluster (dimer) formation occur at all energies, while cluster disruption becomes significant only at $E_{Pt}\geq$20 eV and the formation of residual surface vacancies requires $E_{Pt}\geq$30 eV. We also find that the probability of 3D island formation for small clusters decreases with increasing E_{Pt} due to increased occurrences of atom exchange between layers and the direct incorporation of energetic atoms into clusters.

Thus, the transition that we observe in film growth modes from 3D multilayer to 2D growth at $E_{Pt}\approx$20 eV results from a combination of several irradiation-induced events: increased adatom interlayer migration and decreased 3D cluster formation with increasing E_{Pt}, the onset of significant interlayer adatom migration with $E_{Pt}\geq$15 eV, and the onset of cluster disruption with $E_{Pt}\geq$20 eV. Reduction in island size during film growth leads to a reduced probability for arriving hyperthermal atoms to be deposited on top of islands

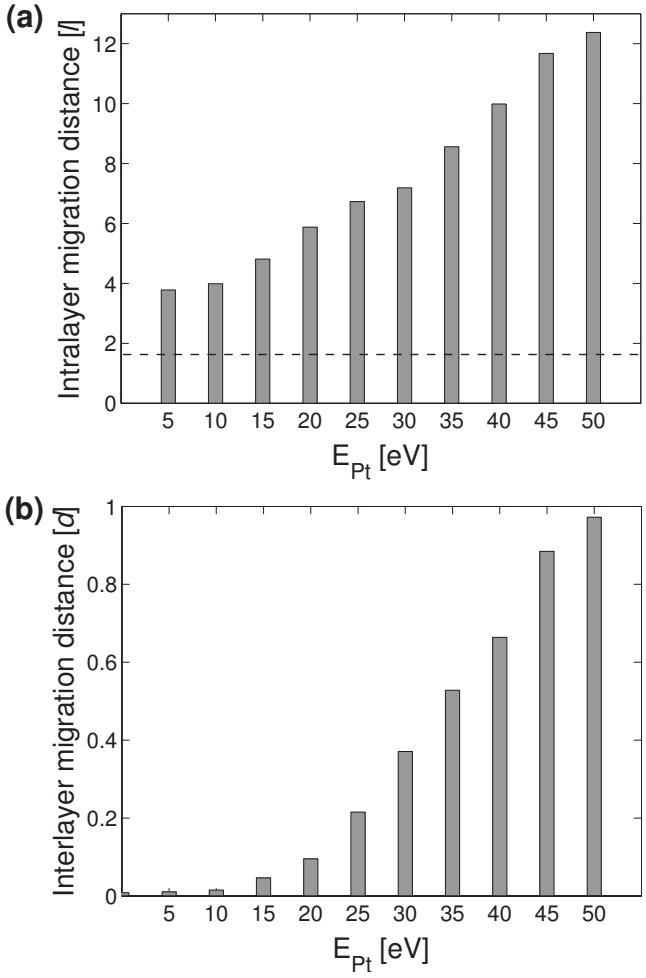

FIG. 3. [(a) and (b)] Average irradiation-induced intra- and interlayer mass transport distances per atom as a function of the incident Pt energy E_{Pt} during deposition on Pt(111). The intra- and interlayer components are expressed in terms of the distance between adjacent fcc and hcp surface sites (l) and the interlayer spacing (d) in the [111] direction. The horizontal dashed line in (a) represents the average intralayer thermal migration distance.

and an increased frequency for already deposited adatoms atop islands to reach island edges and subsequently descend onto the terrace; both effects promote 2D growth.

To proceed a step further, we test the results of our calculations against an inherent limitation of MD simulations for investigating film growth, namely, the use of high fluxes leading to unrealistic deposition rates. In order to probe this effect, we simulated film growth using E_{Pt}=25 eV at a deposition rate of 1 ns^{-1} (a factor of 10 lower than for the previous runs) in a single 1.5-μs-long MD run spanning 1.5 $\times 10^9$ time steps. This deposition rate R is within 2 orders of magnitude of typical experimental values.[24] Diffraction intensity oscillations and plan-view images in Fig. 4, after deposition of 1 and 3 ML, show that near layer-by-layer growth is obtained for deposition rates R of both 1 and 10 ns^{-1}. A comparison of the results shows that higher oscillation amplitudes and smoother surfaces are obtained at the lower R value. This is indeed expected, since a decrease in deposition rate allows longer times for adatoms to sample

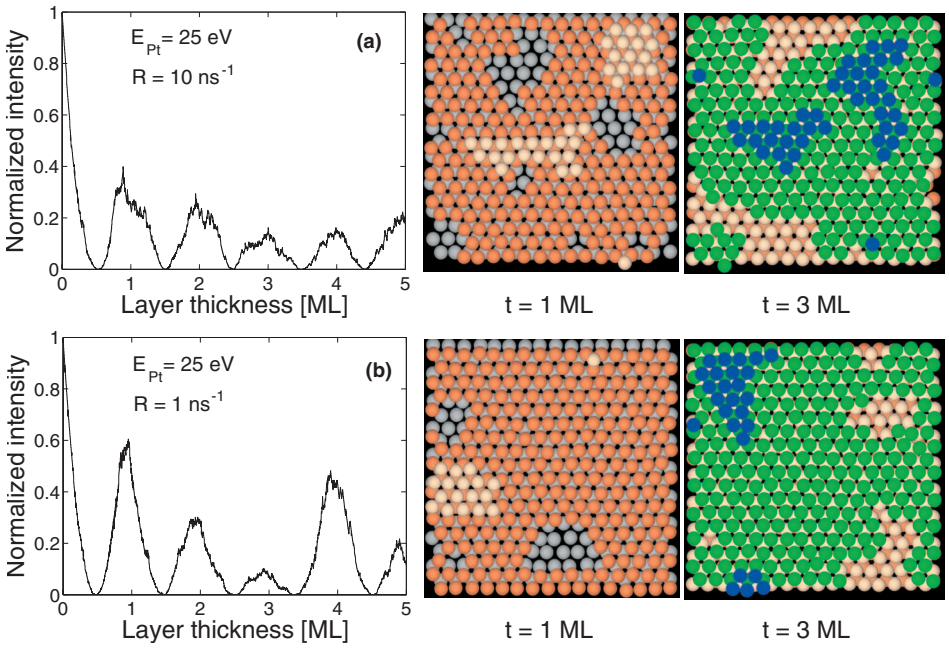

FIG. 4. (Color) Left side: Normalized antiphase diffraction intensity during energetic Pt deposition on Pt(111) with E_{Pt}=25 eV and atom arrival rates R of (a) 10 ns^{-1} and (b) 1 ns^{-1}. Right side: Plan-view images from video files showing the corresponding Pt(111) surface morphology after deposition of 1.0 and 3.0 ML. Substrate surface and first, second, third, and fourth deposited layers are gray, brown, yellow, green, and blue, respectively.

neighboring surface sites before being trapped by subsequently deposited atoms. However, as we discuss below, irradiation-enhanced mass transport effects remain the determinant factor for promoting 2D layer-by-layer growth.

In Fig. 5, we present histograms showing the results for average intralayer and interlayer Pt migration distances for 10 and 100 10 ps time intervals corresponding to the two deposition rates, 10 and 1 ns^{-1}, with E_{Pt}=25 eV. The results clearly demonstrate that even at the lower deposition rate, mass transport is still dominated by events occurring during the first 10 ps.

The important point in Fig. 5 is that the magnitude of irradiation-induced mass transport is essentially unaffected by the deposition rate, while the average thermal intralayer transport distance decreases by approximately two times for the lower flux case. This is a direct consequence of using a more realistic deposition rate. As the time period between incident atom impacts increases by a factor of 10, itinerant thermal adatoms have a higher encounter probability leading to enhanced nucleation which, in turn, decreases the local supersaturation and, hence, the average in-layer migration distance. Similarly, thermal interlayer mass transport, which was already small compared to the number of irradiation-induced interlayer exchanges in the first 10 ps, also decreases by approximately seven times, from 0.0032 to 0.000 46, when using a lower deposition rate [compare the insets in Figs. 5(b) and 5(d)].

TABLE II. Calculated ratios of intra- and interlayer mass transport distances during the first 10 ps following each deposition event with E_{Pt}=25 eV to the total (ρ) and average (r) migration distances over the subsequent 90 and 990 ps for deposition rates R of 10 and 1 ns^{-1}, respectively.

Deposition rate R (ns^{-1})	Intralayer mass transport		Interlayer mass transport	
	ρ_{intra}	r_{intra}	ρ_{inter}	r_{inter}
10	0.47	4.19	7.49	67.57
1	0.10	10.39	4.86	481.15

To further emphasize the role that the first 10 ps time interval plays in the deposition process, we list in Table II the ratios ρ of the intra- and interlayer migration distances over the initial 10 ps intervals to the remaining 90 ps for R =10 ns^{-1} and 990 ps for R=1 ns^{-1}, following each deposition event. As expected, due to the longer time allowed for thermal accommodation, the ratios, which involve *absolute* distances, decrease in value from 0.47 to 0.10 (ρ_{intra}) and from 7.49 to 4.86 (ρ_{inter}). However, the important trend is the *increase* in the ratios r of migration distances in the initial 10 ps to the corresponding average migration distances during the subsequent 90 ps (R=10 ns^{-1}) and 990 ps (R =1 ns^{-1}). The use of a lower deposition flux R results in dramatic increases in both r_{intra}, from 4.2 to 10.4, and r_{inter}, from 67.6 to 481.2. These results represent increases in r_{intra} and r_{inter} by factors of ~2 and 7, which in physical experiments, with deposition rates 2 or more orders of magnitude lower than in our simulations, will be even more dramatic and have particularly significant effects at low deposition temperatures. The results strongly highlight our initial conclusion that irradiation-induced events during the first 10 ps following each deposition event leading to the opening of ion-induced kinetic pathways are key to promoting low-temperature layer-by-layer growth from hyperthermal beams.

IV. CONCLUSIONS

In conclusion, we employ multibillion time step MD simulations to monitor intra- and interlayer mass transport during homoepitaxial growth of Pt(111) from low-energy hyperthermal (E_{Pt}=5–50 eV) Pt atoms and compare the results to growth from thermal beams (E_{Pt}=0.2 eV). Irradiation-induced and thermally activated effects on mass transport rates during deposition are isolated and followed as a func-

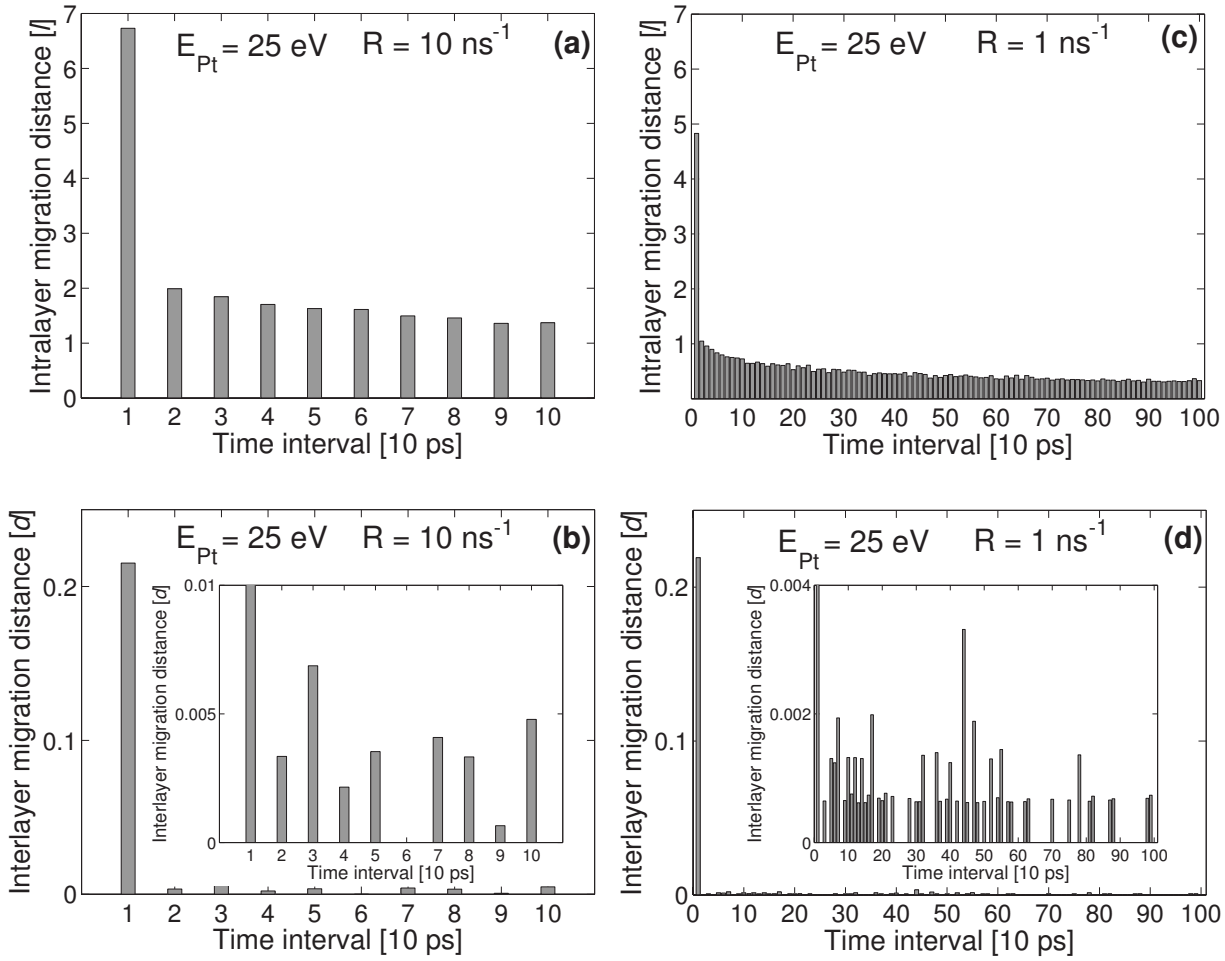

FIG. 5. Average intra- and interlayer mass transport distances plotted as a function of time intervals (10 ps each) between two consecutive impacts during deposition of E_{Pt}=25 eV Pt atoms on Pt(111) with atom arrival rates R of [(a) and (b)] 10 ns^{-1} and [(c) and (d)] 1 ns^{-1}. The intra- and interlayer components are expressed in terms of the distance between adjacent fcc and hcp surface sites (l) and the interlayer spacing (d) in the [111] direction.

tion of time. We observe a transition from 3D multilayer growth toward 2D layer-by-layer growth at $E_{Pt} \sim 20$ eV due to irradiation-induced processes occurring during the first 10 ps following the arrival of each hyperthermal atom. Ion-induced exchange of atoms between layers, direct incorporation of energetic atoms into clusters, and cluster disruption are identified as the primary mechanisms responsible for the transition to layer-by-layer growth. As the deposition rate is decreased closer to typical experimental values, these same kinetic pathways are observed to have an even stronger effect in promoting layer-by-layer growth.

At low temperatures, where thermal migration events are exponentially depressed, the irradiation-induced effects we report here will become increasingly more important. Our results are expected to be valid for most fcc(111) metal films as inferred by the strong similarities observed in their surface properties.[30–32]

ACKNOWLEDGMENTS

The authors acknowledge the financial support given by Swedish Research Council (VR), the Swedish Strategic Research (SSF) Center in Materials Science for Nanoscale Surface Engineering (MS^{2}E), and the U.S. Department of Energy, Division of Materials Science, under Grant No. DEFG02-96ER45439, through the University of Illinois Frederick Seitz Materials Research Laboratory.

[1] J. E. Greene, in *Handbook of Crystal Growth*, edited by D. T. J. Hurle (North-Holland, Amsterdam, 1993), Vol. 1, Pt. A, p. 639.
[2] S. Tungasmita, J. Birch, P. O. Å. Persson, K. Järrendahl, and L. Hultman, Appl. Phys. Lett. **76**, 170 (2000).
[3] N.-E. Lee, G. A. Tomasch, and J. E. Greene, Appl. Phys. Lett. **65**, 3236 (1994).
[4] M. V. Ramana, H. A. Atwater, A. J. Kellock, and J. E. E. Baglin, Appl. Phys. Lett. **62**, 2566 (1993).
[5] D. Gall, I. Petrov, N. Hellgren, L. Hultman, J.-E. Sundgren, and J. E. Greene, J. Appl. Phys. **84**, 6034 (1998).
[6] T.-Y. Lee, S. Kodambaka, J. G. Wen, R. D. Twesten, J. E. Greene, and I. Petrov, Appl. Phys. Lett. **84**, 2796 (2004).
[7] N.-E. Lee, M. Matsouoka, M. R. Sardela, Jr., F. Tian, and J. E. Greene, J. Appl. Phys. **80**, 812 (1996).
[8] The homologous temperature is defined as the ratio of the deposition/substrate temperature (T_s) to the film melting point (T_m) in degrees K. N.-E. Lee, G. Xue, and J. E. Greene, J. Appl. Phys. **80**, 769 (1996).
[9] D. Adamovic, E. P. Münger, V. Chirita, L. Hultman, and J. E. Greene, Appl. Phys. Lett. **86**, 211915 (2005).
[10] D. Adamovic, V. Chirita, E. P. Münger, L. Hultman, and J. E. Greene, Thin Solid Films **515**, 2235 (2006).
[11] M. Villarba and H. Jónsson, Surf. Sci. **324**, 35 (1995).
[12] C. M. Gilmore and J. A. Sprague, Phys. Rev. B **44**, 8950 (1991).
[13] J. Jacobsen, B. H. Cooper, and J. P. Sethna, Phys. Rev. B **58**, 15847 (1998).
[14] X. W. Zhou and H. N. G. Wadley, J. Appl. Phys. **84**, 2301 (1998).
[15] R. A. Johnson, Phys. Rev. B **39**, 12554 (1989).
[16] E. P. Münger, V. Chirita, J. E. Greene, and J.-E. Sundgren, Surf. Sci. **355**, L325 (1996).
[17] K. Kyuno, A. Gölzhäuser, and G. Ehrlich, Surf. Sci. **397**, 191 (1998).
[18] M. Morgenstern, T. Michely, and G. Comsa, Phys. Rev. Lett. **79**, 1305 (1996).
[19] V. Chirita, E. P. Münger, J.-E. Sundgren, and J. E. Greene, Appl. Phys. Lett. **72**, 127 (1998).
[20] V. Chirita, E. P. Münger, J. E. Greene, and J.-E. Greene, Surf. Sci. **436**, L641 (1999).
[21] E. P. Münger, V. Chirita, J.-E. Sundgren, and J. E. Greene, Thin Solid Films **318**, 57 (1998).
[22] V. Chirita, E. P. Münger, J. E. Greene, and J.-E. Sundgren, Thin Solid Films **370**, 179 (2000).
[23] E. P. Münger, V. Chirita, L. Hultman, and J. E. Greene, Surf. Sci. **539**, L567 (2003).
[24] J. Singh and D. E. Wolfe, J. Mater. Sci. **40**, 1 (2005).
[25] P. Desjardins and J. E. Greene, J. Appl. Phys. **79**, 1423 (1996).
[26] T. Michely and J. Cruz, *Islands Mounds, and Atoms: Patterns and Processes in Crystal Growth Far from Equilibrium* (Springer-Verlag, Berlin, 2004).
[27] J. H. Neave, B. A. Joyce, P. J. Dobson, and N. Norton, Appl. Phys. A: Solids Surf. **31**, 1 (1983).
[28] J. M. Van Hove, C. S. Lent, P. R. Pukite, and P. I. Cohen, J. Vac. Sci. Technol. B **1**, 741 (1983).
[29] J. H. Neave, P. J. Dobson, B. A. Joyce, and J. Zhang, Appl. Phys. Lett. **47**, 100 (1985).
[30] K. Kyuno and G. Ehrlich, Surf. Sci. **437**, 29 (1999).
[31] S. C. Wang and G. Ehrlich, Surf. Sci. **239**, 301 (1990).
[32] W. Wulfhekel, N. N. Lipkin, J. Kliewer, G. Rosenfeld, L. C. Jorritsma, B. Poelsema, and G. Comsa, Surf. Sci. **348**, 227 (1996).